HHS Public Access

Author manuscript

*Mol Psychiatry*. Author manuscript; available in PMC 2018 November 01.

Published in final edited form as:

*Mol Psychiatry*. 2017 November ; 22(11): 1512–1519. doi:10.1038/mp.2017.178.

# Molecular basis of dendritic atrophy and activity in stress susceptibility

**TC Francis**[1,4], **R Chandra**[1], **A Gaynor**[1], **P Konkalmatt**[2], **SR Metzbower**[3], **B Evans**[1], **M Engeln**[1], **TA Blanpied**[3], and **MK Lobo**[1]

[1]Department of Anatomy and Neurobiology, University of Maryland School of Medicine, University of Maryland, Baltimore, MD, USA

[2]Division of Renal Diseases and Hypertension, The George Washington University, Washington, DC, USA

[3]Department of Physiology, University of Maryland, University of Maryland, Baltimore, MD, USA

## Abstract

Molecular and cellular adaptations in nucleus accumbens (NAc) medium spiny neurons (MSNs) underlie stress-induced depression-like behavior, but the molecular substrates mediating cellular plasticity and activity in MSN subtypes in stress susceptibility are poorly understood. We find the transcription factor early growth response 3 (EGR3) is increased in D1 receptor containing MSNs of mice susceptible to social defeat stress. Genetic reduction of *Egr3* levels in D1-MSNs prevented depression-like outcomes in stress susceptible mice by preventing D1-MSN dendritic atrophy, reduced frequency of excitatory input and altered *in vivo* activity. Overall, we identify NAc neuronal-subtype molecular control of dendritic morphology and related functional adaptations, which underlie susceptibility to stress.

## INTRODUCTION

Depression affects a significant proportion of the world's population and is currently the leading cause of disability, warranting significant study into the brain mechanisms, which underlie its cause.[1] The nucleus accumbens (NAc) is a critical integration center for emotionally salient information and is a hub for the maintenance of depression-related symptomology.[2–4] Severe, chronic stress, a primary risk factor for depression, causes long-term cellular, molecular, and physiological adaptations to NAc projection neurons, medium spiny neurons (MSNs), in dopamine 1 (D1) and dopamine 2 (D2) receptor expressing subtypes.[5–8] While maintaining many of the same afferents, NAc MSNs project differentially to downstream mesolimbic brain regions. D1-MSNs project to both the ventral

Correspondence: Dr MK Lobo, Department of Anatomy and Neurobiology, University of Maryland School of Medicine, 20 Penn Street, HSF2, Rm 265, Baltimore, MD 21201, USA. mklobo@som.umaryland.edu.

[4]Current address: Synaptic Plasticity Section, National Institute on Drug Abuse Intramural Research Program, Baltimore, MD 21224, USA

**CONFLICT OF INTEREST**

The authors declare no conflict of interest.

Supplementary Information accompanies the paper on the *Molecular Psychiatry* website (http://www.nature.com/mp)

tegmental/substantia nigra and ventral pallidum, and D2-MSNs only project to the ventral pallidum.[9,10] These differences in anatomy, molecular expression, and MSN physiology, which drive differential, often opposing behavioral outcomes in stress, merit significant study into the role of MSN subtypes in depression behaviors.

Electrophysiological recordings demonstrate distinct synaptic and intrinsic alterations in MSN subtypes following stress.[5,6] However, the molecular and cellular mechanisms underlying these adaptations remain elusive. Previous studies have revealed molecular substrates underlying enhanced spine formation and increased frequency of excitatory synaptic transmission following chronic social defeat stress, yet this has not been examined in a cell-type specific manner.[11,12] Similar to these studies, we observed an increase in frequency of excitatory transmission on NAc D2-MSNs.[5] However, we observed a decrease in D1-MSNs,[5] a NAc subtype implicated in the expression of anhedonia, a core behavioral symptom of depression.[6] Additionally, D1-MSN excitability is significantly enhanced by stress.[5] These outcomes indicate stress-driven structural and molecular adaptations are likely specific to MSN subtypes and may dramatically differ between these subtypes.

In this study, we assessed a set of transcription factors, early growth response (EGR) molecules. EGR molecules are downstream of major signaling cascades promoting plasticity in MSNs.[13–17] EGR transcription factors, and EGR3 in particular, mediates neurobiological adaptations of stress and novelty, reward, and social behaviors.[18–23] Additionally, EGR molecules are critically involved in stabilization of neuronal plasticity, neuron outgrowth and cytoskeletal regulation.[16,21,23–25] Chronic stress mediates widespread adaptations to synaptic density and dendritic arbor.[26] Stress-induced impairment in structural and synaptic alterations as well as their molecular underpinnings have been extensively studied in limbic excitatory brain regions,[26–28] but there is minimal information into these mechanisms in GABAergic neurons, including MSN subtypes. Therefore, understanding the nature of these adaptations in the NAc and the causal underlying molecular mechanisms is necessary to parse out stress-induced differences between MSNs. Thus, the EGR proteins are prime candidate molecules to examine the molecular regulation of cellular plasticity in chronic, social stress.

Here we show an EGR family member, EGR3, is necessary to drive susceptibility to stress by controlling stress-driven dendritic morphological adaptations in NAc D1-MSNs. Furthermore, we link stress-induced, EGR3-mediated dendritic changes to functional changes in excitatory synaptic transmission, intrinsic excitability, and *in vivo* cellular activity.

## MATERIALS AND METHODS

### Experimental subjects

D1-Cre (Line FK150)[29] were used for behavioral experiments and electrophysiological recordings. RiboTag (RT) mice ($Rpl22^{tm1.1Psam}/J$)[30] were bred with D1-Cre mice to generate D1-CreXRiboTag (D1-Cre-RT) or D2-Cre mice (Line ER44) to generate D2-CreXRiboTag (D2-Cre-RT) mice used for cell-type-specific gene expression. All mice were bred on a C57Bl6/J background. C57Bl6/J were used for chromatin immunoprecipitation.

CD-1 retired breeders (Charles River, >4 months) were utilized as aggressors. All subjects were male. For all experiments, mice were randomly assigned to experimental groups by cage before surgery and/or treatment. Further, the order of the animals was randomized before behavioral tests. Studies were conducted in accordance with guidelines set up by the IACUC at UMSOM.

### Chronic and subthreshold social defeat stress and sucrose preference

Chronic social defeat stress was performed as previously.[5,31,32] Mice were placed in a large hamster cage containing a novel, aggressive CD-1 retired breeder for 10 min per day. Mice underwent sensory interaction (24 h) across a perforated divider following defeat until the next defeat session. On day 11, social interaction behavior was assessed using video tracking (CleverSys, Reston, VA, USA). Experimental mice were placed in an open field (2.5 min) and assessed for time within an interaction zone around a perforated box. A novel CD-1 was placed in the box and time spent in the interaction zone was measured over 2.5 min. Subthreshold social defeat stress was administered as previously described.[5] Mice were exposed to three distinct CD-1 aggressors for 2 min per defeat session over 1 day with 15 min of sensory contact from the same CD-1 between sessions.

Two-bottle choice sucrose preference was performed following defeat.[5] Mice were habituated for 2 days to two 50 ml bottles filled with water. On the third day, one water bottle was replaced with 0.5% sucrose solution. Water bottles were weighed daily to determine consumption and switched to eliminate side preference. Preference was calculated as percentage of sucrose consumed relative to total liquid consumed.

### Stereotactic viral surgery

Mice were anesthetized with isoflurane. The NAc (from Bregma, anterior/posterior:+1.6, medial/lateral:+/− 1.5, dorsal/ventral: − 4.4) of D1-Cre mice was bilaterally injected with a cre-inducible, double inverted open (DIO)-reading frame adeno-associated virus (AAV) AAV2.5-Ef1a-DIO-Egr3-EYFP (UNC viral vector core)[22] or AAV2.5-Ef1a-DIO-EYFP and AAV2.5-hsyn-DIO-Egr3-miR-mCitrine or AAV2.5-hsyn-DIO-SS-miR-mCitrine.[22] For calcium imaging experiments, mice were co-injected with AAV2.9-flex-GCaMP6f (UPenn Vector Core) and AAV2.2-DIO-Egr3-miR-LacZ or AAV2.2-DIO-SS-miR-LacZ.

### Electrophysiological recordings

No later than 2 weeks after social interaction, isoflurane-anesthetized mice were perfused with oxygenated (95% oxygen, 5% carbon dioxide) iced sucrose artificial cerebrospinal fluid (ACSF) containing (in mM $l^{-1}$): 194 sucrose, 30 NaCl, 26 $NaHCO_3$, 10 Glucose, 4.5 KCl, 3 $MgCl_2$, 1.2 $NaH_2PO_4$, osmolarity 330mOsm. NAc coronal slices (300 μm) were prepared in iced sucrose ACSF. Slices were placed in 33 °C for a 1 h incubation period before recording in incubation ACSF containing (in mM $l^{-1}$): 125 NaCl, 25 $NaHCO_3$, 10 Glucose, 3.5 KCl, 3 $MgCl_2$, 1.25 $NaH_2PO_4$, 0.1 $CaCl_2$. Whole-cell recordings were performed in 33 °C normal ACSF (altered magnesium and calcium: 1 mM $MgCl_2$, 1 mM $CaCl_2$) under DIC visual guidance of a 40 × water-immersion objective (Olympus, Center Valley, PA, USA). Potassium gluconate based internal solution (in mM: 126 K Gluconate, 10 HEPES, 4 KCl, 2 ATP-Mg, 2 $Na_2ATP$, 0.3 GTP, 0.2 EGTA, osmolarity 290–300mOsm) filled patch pipettes

(3–6 MΩ) for all recordings. Signals were amplified (Multiclamp 700B; Molecular Devices, Sunnyvale, CA, USA), acquired (Axoscope 9; Molecular Devices), and digitized at 20 kHz (Digidata 1322; Molecular Devices).

Intrinsic excitability measures were acquired, while dynamically clamping at −75 mV. A pulse-ramp protocol generated by Master9 (AMPI, Jerusalem, Israel) was used to obtain rheobase current. Current (50–300 pA, 500 ms) was injected to determine current-firing frequency relationships across groups. Voltage clamp recordings (−70 mV) to analyze mEPSCs were performed in the presence of 100 μM PTX and 1.5 μM TTX. Series resistance was monitored online. Capacitance was determined by examining charge in capacitive transients with a +5 mV, 500 ms voltage deflection.

### Immunostaining

Mice were perfused with 4% paraformaldehyde, brains were cryoprotected with 30% sucrose, and cryostat (Leica, Buffalo Grove, IL, USA) sectioned at 35 μm. Slices were washed 3 times for 10 min with 1 × phosphate buffered solution (PBS) and blocked in 3% normal donkey serum and 0.3% Triton X (20%) in 1 × PBS. Slices were incubated in rabbit GFP (1:1000; Aves Lab, Tigard, OR, USA; #GFP-1020) and chicken β-Gal (1:250; Promega, #Z3781) primary antibody overnight. Slices were washed 3 times for 15 min and incubated in anti-rabbit Alexa 488 (1:1000; Jackson Immuno, West Grove, PA, USA; #111-545-144) and anti-chicken Cy3 (1:500; Jackson Immuno; #703-165-155) for 2 h followed by PBS washes and mounting with Vectashield DAPI-containing mounting media. Sections were imaged on a B × 61 confocal microscope (Olympus).

### MSN reconstruction and dendrite and spine analysis

Cells were filled with neurobiotin during whole-cell recording and cells were recovered from 5–14 animals per condition. Following recording, brain slices were immediately placed in 4% PFA overnight. The following day, slices were processed by washing 6 times for 15 min per wash in 1 × PBS followed by 5 h of blocking in 10% normal donkey serum and 0.05% Triton X (20%) at room temperature. Slices were incubated in 1:1000 streptavidin-Cy3 (Jackson Immuno; #016-160-084) in blocking solution overnight. Slices were washed 6 times for 10 min and mounted. To analyze dendritic arbor, images were acquired using a *Z*-stack at 2 μm using a 20 × objective at 1.5 × digital zoom. *Z*-stacks were analyzed using the ImageJ (NIH, Bethesda, MD, USA) plugin simple neurite tracer.[33] ImageJ sholl analysis classified concentric ring intersections at 10 μm diameter increments. For spines, 0.2 μm slice Z-stacks were acquired with a 40× objective at 3× digital zoom. Images were deconvolved (ImageJ, NIH) and NeuronStudio (MSSM, CNIC) was used to analyze spine density and classify spines on 2–3 secondary dendrites averaged per animal. For dendrite and spine analysis, the experimenter was blind to the groups.

### Adeno-associated virus construction

Plasmids encoding AAV2.2-DIO-Egr3-miR-IRES-LacZ and AAV2.2-DIO-SS-miR-IRES-LacZ were constructed from AAV2.2-DIO-Egr3-miR-IRES-mCitrine and AAV2.2-DIO-SS-miR-IRES-mCitrine, respectively, as described previously.[22] LacZ was inserted into the vector by replacing the mCitrine. pUC19 vector carrying LacZ sequence (Invitrogen,

Carlsbad, CA, USA) were PCR amplified using Phusion (#M0531S) using primer lacZ forward: (NcoI)5′-CCATGGATGACCATGATTACGCCAA-3′ and lacZ reverse: (BsrGI)5′-TGTACACTATGCGGCATCAGAGCAG-3′, followed by digestion with NcoI and BsrGI restriction enzymes. Purified PCR products were ligated to the destination vector at restriction sites. AAV2.2-DIO-*Egr3*-miR-LacZ and AAV2.2-DIO-SS-miR-LacZ viruses were packaged as described previously using HEK 293 cells: Sigma-Aldrich, St. Louis, MO, USA, #85120602.[22,34] Titers for the AAVs were determined by qRT-PCR as described previously.[34]

### *In vivo* Calcium Imaging

*In vivo* calcium imaging was performed on D1-Cre mice using the Doric miniscope system (Doric, Quebec, QC, Canada). 2mm of brain tissue was aspirated with a constant drip of oxygenated sucrose ACSF before mice were injected with AAV2.9-flex-GCaMP6f within the NAc. A GRIN lens was stereotaxically implanted 100 μm above the injection site. Mice were habituated to the miniscope in their home cage for 5d prior to the first imaging session and 6wks after surgery. Following image registration using the Doric Imaging software and ImageJ background subtraction, a modified constrained nonnegative matrix factorization (CNMF) method and Matlab (MathWorks) script[35] was utilized for deconvolution and extraction of ΔF/F signals. Peak signals were found in ClampFit following extraction utilizing a 2 standard deviation threshold parameter to select events. Signals with half-widths exceeding 3 s were excluded from analysis. Using custom Matlab scripts and TopScan (CleverSys) software, behavioral videos were aligned to calcium images and average frequency and magnitude of ΔF/F peaks were analyzed. For time-locking to interaction events, the segment the segment of time during which mice enter the interaction zone and interact with the novel CD-1 until mice the time point when they leave the interactions zone and stop interacting with the novel CD-1 was extracted. For all cells, calcium activity was averaged across interaction events to find the final waveform presented.

### Cell-type-specific RT RNA Extraction and quantitative (q)RT-PCR

Polyribosome immunoprecipitation was prepared as previously with little modification.[22,30] NAc tissue was collected and pooled from two D1-Cre-RT or D2-Cre-RT mice per sample 24 h after social interaction. Tissue was dounce homogenized in 500 μl buffer containing: 50 mM Tris, 100 mM KCl, 12 mN $MgCl_2$ and 1% NP-40 supplemented with 1 DTT, 100 μg $ml^{-1}$ cyclohexamide, 1 mg $ml^{-1}$ heparin, RNAase, and protein inhibitors (Promega), pH 7.4. Samples were centrifuged to collect supernatant, which was added to the anti-HA antibody (Covance, Princeton, NJ, USA: #MMS-101 R) and incubated overnight at 4 °C with agitator rotation. The following day, 400 μl of protein G magnetic beads (Life Technologies, Carlsbad, CA, USA #100.09D) were added to the lysate and incubated overnight with constant rotation. Magnetic beads were washed in a magnetic rack in high-salt buffer containing (in mM): 50 Tris, 300 KCl, 12 $MgCl_2$, 1 DTT, 1% NP-40, and 100 μg $ml^{-1}$ cyclohexamide, pH 7.4. RNA was quantified with a NanoDrop (Thermo Scientific, Waltham, MA, USA). For qRT-PCR, RNA was extracted using Trizol (Invitrogen) and the MicroElute Total RNA Kit (Omega, Norcross, GA, USA) with a DNase step (Qiagen, Germantown, MD, USA). 400 ng of cDNA was synthesized with iScript cDNA synthesis kit (Bio-Rad, Hercules, CA, USA). cDNA expression changes were measured using qRT-PCR

with Perfecta SYBR Green FastMix (Quanta, Beverly, MA, USA) using the $-\Delta\Delta C_T$ method described previously[5,22,36] compared to GAPDH. qPCR primer sequences can be found in Supplementary Table 1.

### Chromatin Immunoprecipitation

Chromatin immunoprecipitation (ChIP) was performed as previously.[22] A total of 14 gauge NAc punches were collected 24 h after social interaction. Tissue was cross-linked with 1% formaldehyde, and quenched in 2 M glycine prior to freezing at −80 °C. NAc tissue was dounce homogenized in lysis buffer 1c (in mM): 50 HEPES-KOH, 140 NaCl, 1 EDTA, pH 7.5, 10% glycerol, 0.5% NP-40, 0.25% Triton X-100, and protease inhibitors. This step was followed by constant rotation at 4 °C for 10 min and centrifugation at 1350 g for 5 min. Pellets were resuspended in lysis buffer 2 (in mM) 10 Tris, 200 NaCl, 1 EDTA, 0.5 EGTA, and protease inhibitors, and incubated at room temperature for 10 min. Following centrifugation, pellets were resuspended in lysis buffer 3 (in mM): 10 Tris-HCl, 100 NaCl, 1 EDTA, 0.5 EGTA, pH 8.0, 0.1% Nadeoxycholate, 0.5% N-lauroylsarcosine, and protease inhibitors. Chromatin was sheared to 500–700 bp (Diagenode Bioruptor Pico) by 8 cycles of 30 s ON and 30 s OFF. One out of ten volume of 10% Triton X-100 added to each sample to solubilize the membrane and supernatant was collected by centrifugation for 10 min at 20 000 g at 4 °C. A total of 50 μl sample was collected for input. Samples were mixed with beads conjugated to anti-Egr3 rabbit antibody (Santa Cruz, Dallas, TX, USA, #sc-191) or anti-rabbit IgG (Invitrogen; #11202D) for 16 h at 4 °C with constant rotation. Samples were washed with low-salt buffer, high-salt buffer, LiCl wash buffer, 1xTE +50 mM NaCl one time each and feluted in elution buffer by placing in a thermomixter at 65 °C at 1000 r.p.m for 30 min. Samples were centrifuged for 16 000 g for 1 min to collect the supernatant. Samples and inputs underwent reverse cross-linking at 65 °C overnight, followed by DNA purification (Qiagen PCR purification kit). Samples were normalized to input controls and compared with IgG samples for qPCR analysis. The primer sequences for ChIP samples can be found in Supplementary Table 1.

### Statistical analysis

Graphpad Prism 5.0 software was used for statistical analysis. All statistics can be found in Supplementary Table 2. Interaction effects are reported, unless noted. For ANOVA tests, Bonferroni post *hoc* tests were used. In figure legends: $*P<0.05$, $**P<0.01$, $***P<0.001$, $****P<0.0001$. All graphs represent mean ± s.e. Sample sizes were determined from previous studies using chronic or subthreshold defeat.[5] Grubbs outlier test was performed on the data with obvious outliers and no more than one animal or sample was removed per group. Individual values are plotted in all graphs to report variation and variance is similar between groups that are statistically compared.

## RESULTS

### D1-MSN *Egr3* expression mediates susceptibility to defeat

Expression of *Egr1-4* was examined using NAc cell-type-specific analysis in mice susceptible or resilient to defeat. We utilized D1-Cre-RT and D2-Cre-RT mice allowing for translational profiling of ribosome-associated mRNAs specifically from D1-MSN or D2-

MSN subtypes (Figure 1a).[22,30] Mice underwent 10 days of defeat, resulting in susceptible and resilient cohorts (Supplementary Figure S1a) and NAc tissue punches were collected 24 h after social interaction behavior. D1-MSN *Egr3* and *Egr1* expression was increased in susceptible mice and resilient mice, respectively, compared to non-defeated mice (Figure 1b, Supplementary Figure S1b). D2-MSNs from susceptible animals display reduced expression of *Egr4*, but no change in *Egr3* was observed (Figure 1b, Supplementary Figure S1b). D1-MSN, but not D2-MSN *Egr3* expression negatively correlated with social interaction time (Supplementary Figure S1c). No correlation was observed between *Egr1* and interaction time (Supplementary Figure S1d). Therefore, we focused on D1-MSN EGR3 for the remainder of the study. To examine the effects of D1-MSN *Egr3* overexpression (*Egr3*-OE) on susceptibility, a DIO-AAV[22] was injected into the NAc of D1-Cre mice (Figure 1c; Supplementary Figure S1e). *Egr3*-OE D1-Cre mice were subjected to a 1 day subthreshold defeat, which does not normally result in depression-like behavior.[5] However, D1-MSN *Egr3*-OE reduced interaction time with a novel target mouse compared to defeat EYFP and non-defeated controls (Figure 1d), without affecting locomotor behaviors (Supplementary Figure S1f), suggesting D1-MSN *Egr3* overexpression promotes stress susceptibility. Next, we used a DIO-AAV *Egr3*-microRNA (*Egr3*-miR)[22] to knockdown NAc D1-MSN *Egr3* expression, by injecting into the NAc of D1-Cre mice (Figure 1c, Supplementary Figure S1g). D1-MSN expression of *Egr3*-miR, but not a scrambled sequence microRNA (SS-miR), was sufficient to block social avoidance (Figure 1e) and prevent reduced sucrose preference (Figure 1f) without affecting locomotion (Supplementary Figure S1h). Therefore, NAc D1-MSN *Egr3* expression is necessary to modify depression-like behavioral outcomes to social defeat stress.

### Stress and *Egr3* regulates excitatory transmission on D1-MSN but not spine density

Following stress, excitatory transmission on NAc D1-MSNs is reduced.[5] *Egr3*-miR in D1-MSNs was sufficient to prevent the miniature excitatory postsynaptic current (mEPSC) frequency reduction caused by defeat in SS-miR defeat (Figure 2a). Surprisingly, while stress did not alter the total density of spines in D1-MSNs, Egr3 knockdown and stress together, enhanced total spine density (Figure 2b), thin, and stubby spine density (Figure 2c). These results suggested an alternative mechanism changes mEPSC frequency, perhaps through alterations in the total synapse number.

### *Egr3* knockdown blocks stress-induced dendritic atrophy

We found a reduction in D1-MSN rheobase current positively correlated with social interaction time and enhanced spiking to injected current in SS-miR-stressed mice (Figure 3a, Supplementary Figure 2a)[5,8] and was blocked by D1-MSN *Egr3* knockdown (Figure 3a). Increased input resistance, after stress, was also blocked by D1-MSN *Egr3*-miR knockdown (Figure 3b). Alterations in input resistance and excitability in SS-miR defeat, mice were likely controlled in part by a reduced inward rectification, a function of inward rectifying potassium channels, in defeated mice (Supplementary Figure 2b). Interestingly, capacitance was reduced by defeat and blocked by *Egr3* knockdown (Figure 3c). These alterations suggest EGR3-mediated dendritic structural change can facilitate the reduction in excitatory transmission by a loss in total number of synapses.

To determine whether EGR3 mediates dendritic structural changes in response to stress, we examined dendritic morphology of D1-MSNs following stress from neurobiotin-filled cells during whole-cell recordings. Sholl analysis uncovered a reduction in concentric ring intersections in D1-Cre SS-miR-defeated mice, while *Egr3*-miR enhanced overall intersections (Figure 3d). We observed a reduction in NAc D1-MSN total dendritic length from defeat SS-miR mice, which was blocked by *Egr3*-miR (Figure 3e). Furthermore, the number of dendritic branch points was increased by *Egr3* knockdown relative to all groups (Figure 3f). No changes were observed in soma diameter (Supplementary Figure 2c).

### *EGR3* transcriptionally regulates dendritic structural molecules in susceptible mice

To explore molecules controlled by EGR3, we used ChIP with an EGR3 antibody to examine Egr3 binding to gene promoters involved in regulation of dendritic morphology and plasticity. ChIP mice displayed significantly reduced time in the interaction zone after social defeat stress (Figure 4a). EGR3 displayed increased binding to the promoter of *RhoA*, a gene involved in negative regulation of dendritic structure[37] and to *Actn1*, an actin-associated gene (Figure 4b). Furthermore, EGR3 binding to the *Shank2* promoter, a gene involved in regulating dendritic morphology and cognitive behavior,[38] was decreased.

### Stress alters D1-MSN activity *in vivo*

To determine the effects of chronic stress-induced physiological and morphological changes on D1-MSN activity *in vivo*, we next sought to examine GCaMP-mediated calcium activity in D1-MSNs in SS-miR and *Egr3*-miR conditions during social interaction. To test this, AAV-DIO-*Egr3*-miR-LacZ or AAV-DIO-SS-miR-LacZ was co-injected with AAV-DIO-GCaMP6f in the NAc of D1-Cre mice to reduce NAc *Egr3* expression or as a control, respectively (Supplementary Figures 3a, b). A chronically implantable gradient-index (GRIN) lens[39–41] was inserted in the NAc (Figure 5a) to observe calcium transients *in vivo* (Figure 5b Supplementary Movies 1 and 2). No differences were observed in frequency of calcium transients when mice were outside of the interaction zone (Supplementary Figure 3c) or when frequency was examined across the entire session (Supplementary Figure 3d). The results agree with observations that MSNs are largely quiescent under resting conditions.[42] In agreement with this finding, average calcium signals were increased during social interaction (Supplementary Figure 3e). Defeated SS-miR mice displayed reduced interaction time in the target condition only, while all *Egr3*-miR-injected mice displayed normal social interaction (Figure 5c, Supplementary Figure 3f, h). The frequency of calcium transients in D1-MSNs of SS-miR mice was significantly reduced compared to *Egr3*-miR mice following social defeat stress in the target condition only (Figure 5d, Supplementary Figures 3g, i). When frequency was examined from all individual cells, only SS-miR mouse cells showed a significant decrease in frequency after defeat, while cells from *Egr3*-miR mice displayed no change (Supplementary Figures 3j–k). Taken together, these results indicate EGR3 is necessary for defeat-induced reduction in *in vivo* activity.

We next examined the calcium transient magnitude in D1-MSNs during social interaction time-locked to the start or end of an interaction event. Overall, the average ΔF/F calcium signal was enhanced in *Egr3*-miR mice, suggesting a baseline increase in the magnitude of neural activity (Supplementary Figure 4a). Individual calcium signals were normalized to

the 1 s period prior to or after a social interaction bout and individual cells were averaged across multiple interaction events. Prior to defeat, no difference was observed in the average amplitude of calcium transients (Figure 5e, Supplementary Table 3). Following defeat, only SS-miR mice displayed increased calcium activity beginning 1.1 s following the start of social interaction bouts, which peaked at 1.3 s (Figure 5e, Supplementary Figure 4b, Supplementary Table 3). SS-miR mice displayed a significant increase in calcium transient amplitude 4.1 s prior to termination of social interaction bouts following defeat only (Supplementary Figure 4c, Supplementary Table 4), likely corresponding to the beginning of the interaction bout, as the average interaction time for SS-miR mice during individual bouts following defeat was 6 s (Supplementary Figure 4d).

## DISCUSSION

To our knowledge, our studies demonstrate for the first time that the transcription factor EGR3 plays a major role in stress susceptibility by inducing dendritic atrophy in NAc D1-MSNs. Widespread changes in excitatory activity, dendritic arbor and loss of spines throughout the brain following stress and depression have been documented in excitatory brain regions.[27] Loss of arbor complexity in these regions also reduces excitatory transmission via a total loss in synapses, consistent with our NAc findings. However, spine changes were not observed in defeated mice,[11,12] suggesting these changes may be specific to D2-MSNs. Further, activation of excitatory regions such as the prefrontal cortical circuit to the NAc restores normal social interaction and sucrose preference.[43] Indeed, deep brain stimulation of the NAc and targeted prefrontal-cortical stimulation in humans is antidepressant,[44,45] suggesting stimulation may compensate for the loss or cause morphological changes to alleviate depression.

Our calcium imaging data, revealing a decrease in D1-MSN activity in susceptible animals is consistent with reduced synaptic input that drives stress-induced anhedonia[5,6] and enhanced activity in D1-MSNs in pro-reward and reinforcement outcomes.[5,6,36,46–48] The reduction in synaptic input in susceptible mice is unlikely due to an alteration in the density of synapses, but rather a consequence of a loss in the total number of synapses, which is driven by dendritic loss following stress. Interestingly, the enhanced intrinsic excitability we observed in D1-MSNs of defeated mice does not result in enhanced frequency of D1-MSN *in vivo* activity during social interaction. Rather, intrinsic excitability appears to play a role in enhancing the strength of the calcium signal in D1-MSNs following initiation of social interaction behavior in mice susceptible to social defeat stress. It is well established that neurons actively balances input and output.[49] Thus, the intrinsic excitability change may reflect an EGR3-mediated homeostatic mechanism to maintain equal strength of activity in the face of reduced excitatory transmission due to a reduction in the total number of synapses occurring through stress-induced dendritic atrophy.[49,50] Our calcium imaging data suggest the enhancement in excitability provides a stronger, more salient signal on D1-MSNs despite overall reduced excitatory input frequency. Therefore, following defeat, when salient stimuli activate D1-MSNs, the probability of activating cells may be increased, despite reduced basal activity.

Overall, we provide a new understanding of the molecular mechanisms occurring in NAc D1-MSNs that lead to altered cellular and physiological adaptations, and ultimately drive stress susceptible behavior. Many of these changes are consistent with changes found in other brain regions. Identifying these mechanisms has potential benefit for development of therapeutic treatment for stress-related behaviors such as depression.

## Supplementary Material

Refer to Web version on PubMed Central for supplementary material.

## Acknowledgments

We thank Brian N. Mathur and Scott M. Thompson (UMSOM) for input on electrophysiology experiments. This work was supported by NIMH R01MH106500, NIDA R01DA038613 and The One Mind/Janssen Rising Star Translational Research Award.

## References

1. Ferrari AJ, Charlson FJ, Norman RE, Patten SB, Freedman G, Murray CJ, et al. Burden of depressive disorders by country, sex, age, and year: Findings from the global burden of disease study 2010. PLoS Med. 2013; 10:e1001547. [PubMed: 24223526]
2. Krishnan V, Nestler EJ. The molecular neurobiology of depression. Nature. 2008; 455:894–902. [PubMed: 18923511]
3. Russo SJ, Nestler EJ. The brain reward circuitry in mood disorders. Nat Rev Neurosci. 2013; 14:609–625. [PubMed: 23942470]
4. Floresco SB. The nucleus accumbens: an interface between cognition, emotion, and action. Annu Rev Psychol. 2015; 66:25–52. [PubMed: 25251489]
5. Francis TC, Chandra R, Friend DM, Finkel E, Dayrit G, Miranda J, et al. Nucleus accumbens medium spiny neuron subtypes mediate depression-related outcomes to social defeat stress. Biol Psychiatry. 2015; 77:212–222. [PubMed: 25173629]
6. Lim BK, Huang KW, Grueter BA, Rothwell PE, Malenka RC. Anhedonia requires MC4R-mediated synaptic adaptations in nucleus accumbens. Nature. 2012; 487:183–189. [PubMed: 22785313]
7. Dias C, Feng J, Sun H, Shao NY, Mazei-Robison MS, Damez-Werno D, et al. Beta-catenin mediates stress resilience through Dicer1/microRNA regulation. Nature. 2014; 516:51–55. [PubMed: 25383518]
8. Francis TC, Lobo MK. Emerging role for nucleus accumbens medium spiny neuron subtypes in depression. Biol Psychiatry. 2016; 81:645–653. [PubMed: 27871668]
9. Smith RJ, Lobo MK, Spencer S, Kalivas PW. Cocaine-induced adaptations in D1 and D2 accumbens projection neurons (a dichotomy not necessarily synonymous with direct and indirect pathways). Curr Opin Neurobiol. 2013; 23:546–552. [PubMed: 23428656]
10. Kupchik YM, Brown RM, Heinsbroek JA, Lobo MK, Schwartz DJ, Kalivas PW. Coding the direct/indirect pathways by D1 and D2 receptors is not valid for accumbens projections. Nat Neurosci. 2015; 18:1230–1232. [PubMed: 26214370]
11. Golden SA, Christoffel DJ, Heshmati M, Hodes GE, Magida J, Davis K, et al. Epigenetic regulation of RAC1 induces synaptic remodeling in stress disorders and depression. Nat Med. 2013; 19:337–344. [PubMed: 23416703]
12. Christoffel DJ, Golden SA, Dumitriu D, Robison AJ, Janssen WG, Ahn HF, et al. IkappaB kinase regulates social defeat stress-induced synaptic and behavioral plasticity. J Neurosci. 2011; 31:314–321. [PubMed: 21209217]
13. Kim JH, Roberts DS, Hu Y, Lau GC, Brooks-Kayal AR, Farb DH, et al. Brain-derived neurotrophic factor uses CREB and Egr3 to regulate NMDA receptor levels in cortical neurons. J Neurochem. 2012; 120:210–219. [PubMed: 22035109]

14. Roberts DS, Hu Y, Lund IV, Brooks-Kayal AR, Russek SJ. Brain-derived neurotrophic factor (BDNF)-induced synthesis of early growth response factor 3 (Egr3) controls the levels of type A GABA receptor alpha 4 subunits in hippocampal neurons. J Biol Chem. 2006; 281:29431–29435. [PubMed: 16901909]
15. Li L, Carter J, Gao X, Whitehead J, Tourtellotte WG. The neuroplasticity-associated arc gene is a direct transcriptional target of early growth response (egr) transcription factors. Mol Cell Biol. 2005; 25:10286–10300. [PubMed: 16287845]
16. Li L, Yun SH, Keblesh J, Trommer BL, Xiong H, Radulovic J, et al. Egr3, a synaptic activity regulated transcription factor that is essential for learning and memory. Mol Cell Neurosci. 2007; 35:76–88. [PubMed: 17350282]
17. Thiel G, Mayer SI, Muller I, Stefano L, Rossler OG. Egr-1- A ca(2+)-regulated transcription factor. Cell Calcium. 2010; 47:397–403. [PubMed: 20303171]
18. Milbrandt J. A nerve growth factor-induced gene encodes a possible transcriptional regulatory factor. Science. 1987; 238:797–799. [PubMed: 3672127]
19. Malkani S, Rosen JB. Specific induction of early growth response gene 1 in the lateral nucleus of the amygdala following contextual fear conditioning in rats. Neuroscience. 2000; 97:693–702. [PubMed: 10842014]
20. Bhat RV, Worley PF, Cole AJ, Baraban JM. Activation of the zinc finger encoding gene krox-20 in adult rat brain: Comparison with zif268. Brain Res Mol Brain Res. 1992; 13:263–266. [PubMed: 1317498]
21. Gallitano-Mendel A, Izumi Y, Tokuda K, Zorumski CF, Howell MP, Muglia LJ, et al. The immediate early gene early growth response gene 3 mediates adaptation to stress and novelty. Neuroscience. 2007; 148:633–643. [PubMed: 17692471]
22. Chandra R, Francis TC, Konkalmatt P, Amgalan A, Gancarz AM, Dietz DM, et al. Opposing role for Egr3 in nucleus accumbens cell subtypes in cocaine action. J Neurosci. 2015; 35:7927–7937. [PubMed: 25995477]
23. O'Donovan KJ, Tourtellotte WG, Millbrandt J, Baraban JM. The EGR family of transcription-regulatory factors: Progress at the interface of molecular and systems neuroscience. Trends Neurosci. 1999; 22:167–173. [PubMed: 10203854]
24. Jones MW, Errington ML, French PJ, Fine A, Bliss TV, Garel S, et al. A requirement for the immediate early gene Zif268 in the expression of late LTP and long-term memories. Nat Neurosci. 2001; 4:289–296. [PubMed: 11224546]
25. Quach DH, Oliveira-Fernandes M, Gruner KA, Tourtellotte WG. A sympathetic neuron autonomous role for Egr3-mediated gene regulation in dendrite morphogenesis and target tissue innervation. J Neurosci. 2013; 33:4570–4583. [PubMed: 23467373]
26. McEwen BS. Physiology and neurobiology of stress and adaptation: Central role of the brain. Physiol Rev. 2007; 87:873–904. [PubMed: 17615391]
27. McEwen BS, Bowles NP, Gray JD, Hill MN, Hunter RG, Karatsoreos IN, et al. Mechanisms of stress in the brain. Nat Neurosci. 2015; 18:1353–1363. [PubMed: 26404710]
28. Herman JP, Ostrander MM, Mueller NK, Figueiredo H. Limbic system mechanisms of stress regulation: Hypothalamo-pituitary-adrenocortical axis. Prog Neuropsychopharmacol Biol Psychiatry. 2005; 29:1201–1213. [PubMed: 16271821]
29. Gong S, Doughty M, Harbaugh CR, Cummins A, Hatten ME, Heintz N, et al. Targeting cre recombinase to specific neuron populations with bacterial artificial chromosome constructs. J Neurosci. 2007; 27:9817–9823. [PubMed: 17855595]
30. Sanz E, Yang L, Su T, Morris DR, McKnight GS, Amieux PS. Cell-type-specific isolation of ribosome-associated mRNA from complex tissues. Proc Natl Acad Sci USA. 2009; 106:13939–13944. [PubMed: 19666516]
31. Berton O, McClung CA, Dileone RJ, Krishnan V, Renthal W, Russo SJ, et al. Essential role of BDNF in the mesolimbic dopamine pathway in social defeat stress. Science. 2006; 311:864–868. [PubMed: 16469931]
32. Krishnan V, Han MH, Graham DL, Berton O, Renthal W, Russo SJ, et al. Molecular adaptations underlying susceptibility and resistance to social defeat in brain reward regions. Cell. 2007; 131:391–404. [PubMed: 17956738]

33. Longair MH, Baker DA, Armstrong JD. Simple neurite tracer: Open source software for reconstruction, visualization and analysis of neuronal processes. Bioinformatics. 2011; 27:2453–2454. [PubMed: 21727141]
34. Prasad KM, Smith RS, Xu Y, French BA. A single direct injection into the left ventricular wall of an adeno-associated virus 9 (AAV9) vector expressing extracellular superoxide dismutase from the cardiac troponin-T promoter protects mice against myocardial infarction. J Gene Med. 2011; 13:333–341. [PubMed: 21674736]
35. Pnevmatikakis EA, Soudry D, Gao Y, Machado TA, Merel J, Pfau D, et al. Simultaneous denoising, deconvolution, and demixing of calcium imaging data. Neuron. 2016; 89:285–299. [PubMed: 26774160]
36. Lobo MK, Covington HE 3rd, Chaudhury D, Friedman AK, Sun H, Damez-Werno D, et al. Cell type-specific loss of BDNF signaling mimics optogenetic control of cocaine reward. Science. 2010; 330:385–390. [PubMed: 20947769]
37. Chen H, Firestein BL. RhoA regulates dendrite branching in hippocampal neurons by decreasing cypin protein levels. J Neurosci. 2007; 27:8378–8386. [PubMed: 17670984]
38. Berkel S, Tang W, Trevino M, Vogt M, Obenhaus HA, Gass P, et al. Inherited and de novo SHANK2 variants associated with autism spectrum disorder impair neuronal morphogenesis and physiology. Hum Mol Genet. 2012; 21:344–357. [PubMed: 21994763]
39. Cai DJ, Aharoni D, Shuman T, Shobe J, Biane J, Song W, et al. A shared neural ensemble links distinct contextual memories encoded close in time. Nature. 2016; 534:115–118. [PubMed: 27251287]
40. Ghosh KK, Burns LD, Cocker ED, Nimmerjahn A, Ziv Y, Gamal AE, et al. Miniaturized integration of a fluorescence microscope. Nat Methods. 2011; 8:871–878. [PubMed: 21909102]
41. Resendez SL, Jennings JH, Ung RL, Namboodiri VM, Zhou ZC, Otis JM, et al. Visualization of cortical, subcortical and deep brain neural circuit dynamics during naturalistic mammalian behavior with head-mounted microscopes and chronically implanted lenses. Nat Protoc. 2016; 11:566–597. [PubMed: 26914316]
42. Bolam JP, Hanley JJ, Booth PA, Bevan MD. Synaptic organisation of the basal ganglia. J Anat. 2000; 196(Pt 4):527–542. [PubMed: 10923985]
43. Vialou V, Bagot RC, Cahill ME, Ferguson D, Robison AJ, Dietz DM, et al. Prefrontal cortical circuit for depression- and anxiety-related behaviors mediated by cholecystokinin: Role of DeltaFosB. J Neurosci. 2014; 34:3878–3887. [PubMed: 24623766]
44. Schlaepfer TE, Cohen MX, Frick C, Kosel M, Brodesser D, Axmacher N, et al. Deep brain stimulation to reward circuitry alleviates anhedonia in refractory major depression. Neuropsychopharmacology. 2008; 33:368–377. [PubMed: 17429407]
45. George MS, Wassermann EM, Williams WA, Callahan A, Ketter TA, Basser P, et al. Daily repetitive transcranial magnetic stimulation (rTMS) improves mood in depression. Neuroreport. 1995; 6:1853–1856. [PubMed: 8547583]
46. Calipari ES, Bagot RC, Purushothaman I, Davidson TJ, Yorgason JT, Pena CJ, et al. In vivo imaging identifies temporal signature of D1 and D2 medium spiny neurons in cocaine reward. Proc Natl Acad Sci USA. 2016; 113:2726–2731. [PubMed: 26831103]
47. Gunaydin LA, Grosenick L, Finkelstein JC, Kauvar IV, Fenno LE, Adhikari A, et al. Natural neural projection dynamics underlying social behavior. Cell. 2014; 157:1535–1551. [PubMed: 24949967]
48. Kravitz AV, Tye LD, Kreitzer AC. Distinct roles for direct and indirect pathway striatal neurons in reinforcement. Nat Neurosci. 2012; 15:816–818. [PubMed: 22544310]
49. Turrigiano GG. The self-tuning neuron: synaptic scaling of excitatory synapses. Cell. 2008; 135:422–435. [PubMed: 18984155]
50. Pratt KG, Aizenman CD. Homeostatic regulation of intrinsic excitability and synaptic transmission in a developing visual circuit. J Neurosci. 2007; 27:8268–8277. [PubMed: 17670973]

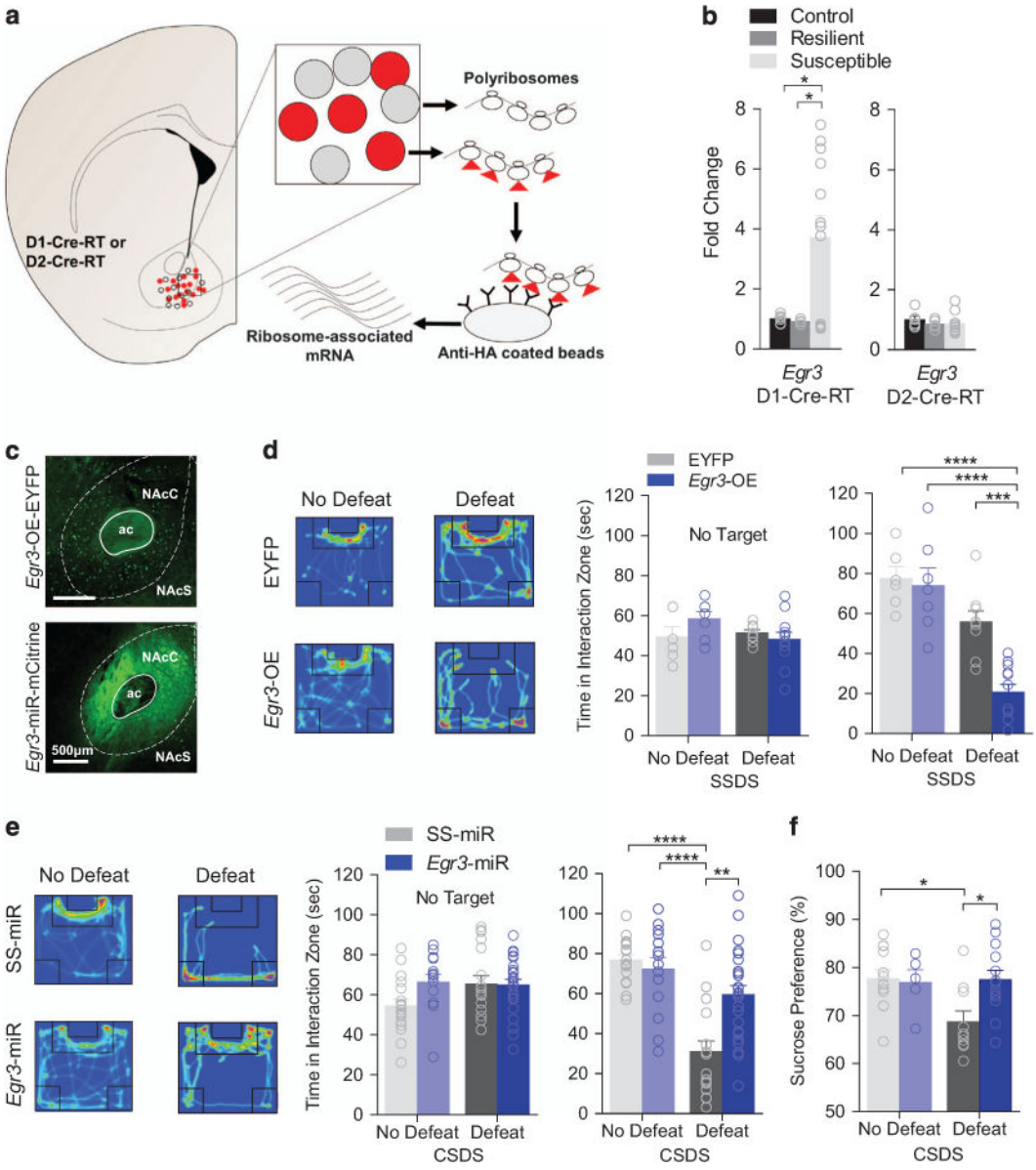


**Figure 1.**

D1-MSN *Egr3* expression controls susceptibility to social defeat stress. (**a**) Schematic of the RiboTag method for NAc MSN-specific isolation of ribosome-associated RNA. HA-tags are expressed on ribosomes in a Cre-dependent manner in MSN subtypes (red). RNA is extracted and isolated from D1-MSNs or D2-MSNs by immunoprecipation by utilizing anti-HA-tagged magnetic beads. (**b**) *Egr3* is upregulated in D1-MSNs of susceptible mice ($P<0.05$, $n = 5–10$ samples per group). *Egr3* remains unchanged in D2-MSNs across all phenotypes ($P>0.05$, $n = 5–10$ samples per group). (**c**) Representative *Egr3*-OE-EYFP or *Egr3*-miR-mCitrine NAc D1-MSN expression. (**d**) Heatmaps displaying mouse movement within the open field during the presence of a novel target mouse are featured for defeated mice. Warm colors indicate more time is spent in an area and cool colors indicate less time. NAc D1-MSN *Egr3*-OE reduces time mice spent in the interaction zone after subthreshold

defeat (Target $P<0.01$; No target, $P>0.05$; $n = 6–12$ mice per group). (**e**) D1-MSNs *Egr3*-miR blocks defeat-induced social aversion (Target $P<0.001$; No Target $P>0.05$; $n = 12–22$ mice per group). (**f**) *Egr3*-miR in D1-MSNs blocks the stress-induced reduction in sucrose preference ($P<0.05$; $n = 6–12$ mice per group). Exact statistics can be found in Supplementary Table 1.

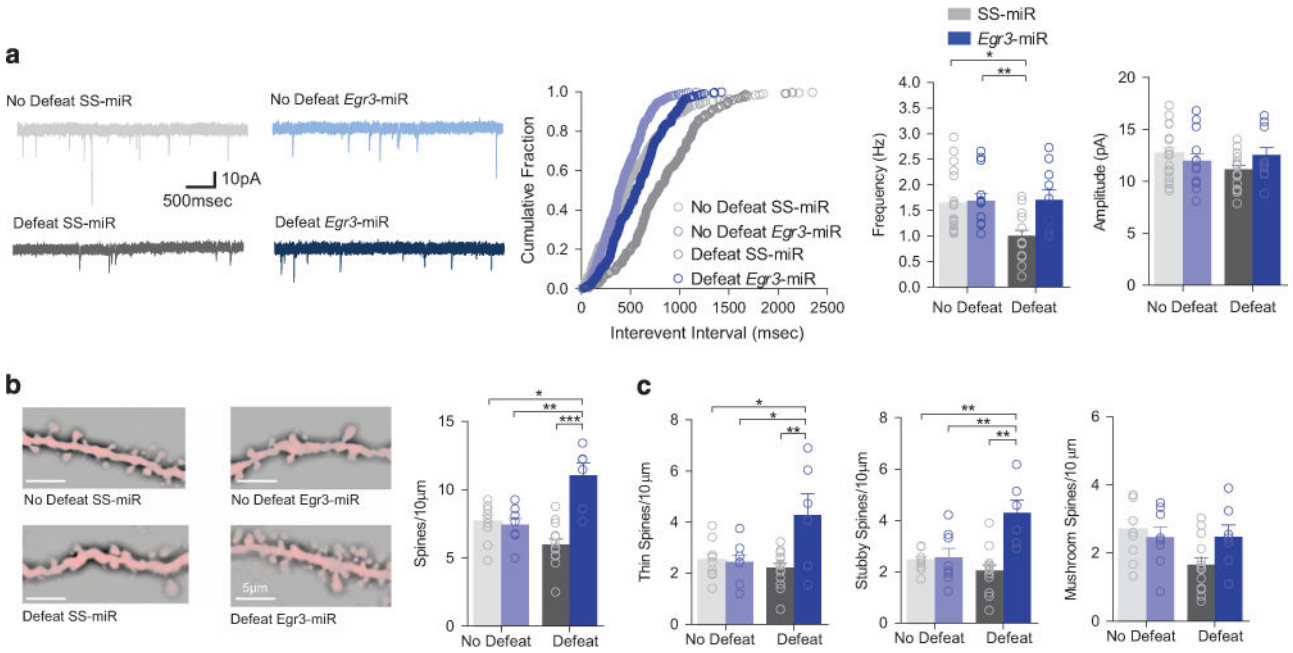


**Figure 2.**

D1-MSN-specific knockdown of *Egr3* prevents stress-induced changes in mEPSC frequency. (**a**) A cumulative probability plot shows a significant rightward shift in the distribution of inter-event intervals for mEPSCs in susceptible mice (No defeat SS-miR vs Defeat SS-miR, $P<0.0001$). mEPSC frequency significantly decreased by defeat was blocked by Egr3-miR (virus, $P<0.01$, defeat, $P<0.05$, $N(n) = 3–4(10–20)$) and mEPSC amplitude remained unchanged by defeat or Egr3-miR ($P>0.05$, Mice(cells), $N(n) = 3–4(10–20)$). (**b**) Representative dendrites are shown. Total density of spines was increased in D1-MSN Egr3-miR-defeated mice ($P<0.0001$; 5–14 mice per group). (**c**) Thin spine density ($P<0.01$; 5–14 mice per group) and stubby spine density ($P<0.01$; 5–14 mice per group) were increased by Egr3-miR and defeat. Mushroom spine density remained unchanged ($P>0.05$; 5–14 mice per group). Exact statistics can be found in Supplementary Table 1.

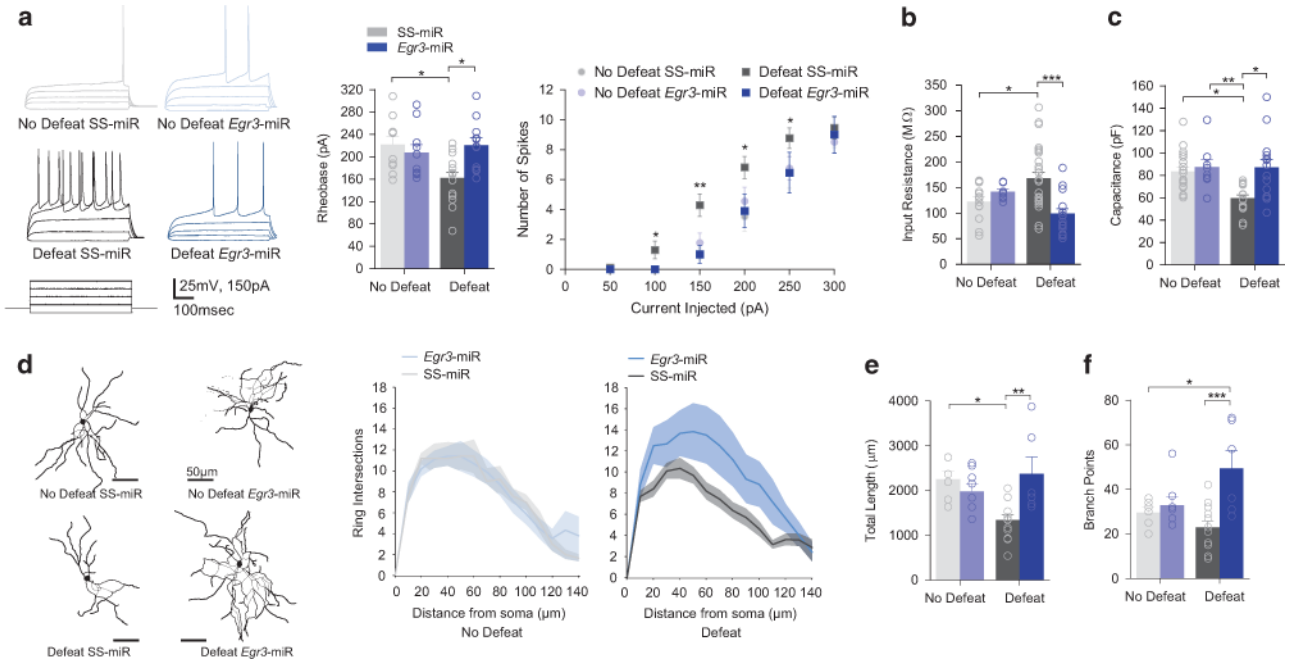


**Figure 3.**

D1-MSN-specific knockdown of *Egr3* prevents stress-induced excitability enhancements and morphological changes. (**a**) Decreased rheobase by defeat was blocked by *Egr3*-miR ($P<0.05$; $N(n)$ = 3–6(10–21) per group) and enhanced spiking using was also blocked by *Egr3* knockdown. (**b**) Defeat-induced input resistance changes were blocked by *Egr3* knockdown ($P<0.01$; $N(n)$ = 3–6(11–28) per group). (**c**) Defeat decreased capacitance was blocked by *Egr3* knockdown ($P<0.05$; $N(n)$ = 3–6(11–28) per group (**d**) Representative skeleton diagrams are shown. The number of concentric ring intersections is decreased following defeat ($P<0.001$). (**e**) The total dendritic length is reduced by defeat and restored by D1-MSN *Egr3* knockdown ($P<0.01$; 6–8 mice per group). (**f**) Branch points are increased by D1-MSN *Egr3*-miR and defeat ($P<0.05$; 6–8 mice per group). Exact statistics can be found in Supplementary Table 1.

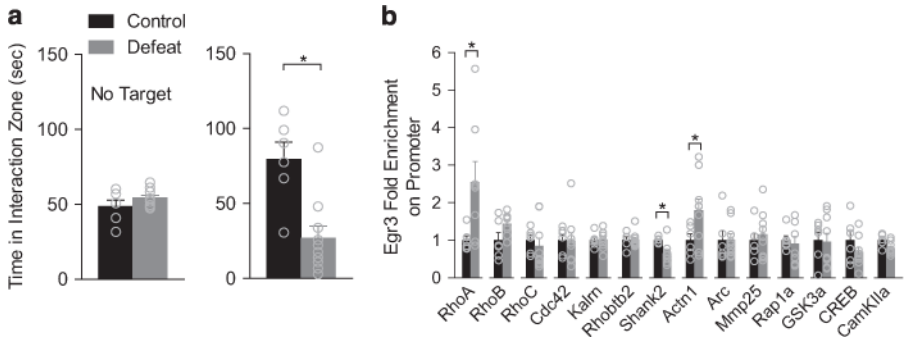


**Figure 4.**

EGR3 binding to cytoskeletal-related promoters is altered by defeat. (**a**) Mice used for ChIP analysis showed significantly reduced time in the interaction zone following defeat ($P<0.05$, $n = 6–10$ pooled mice). (**b**) EGR3 displayed increase binding to the promoters of *RhoA* ($P<0.05$) and *Actn1* ($P<0.05$) and decreased binding to the promoter of *Shank2* ($P<0.05$). Exact statistics can be found in Supplementary Table 1.

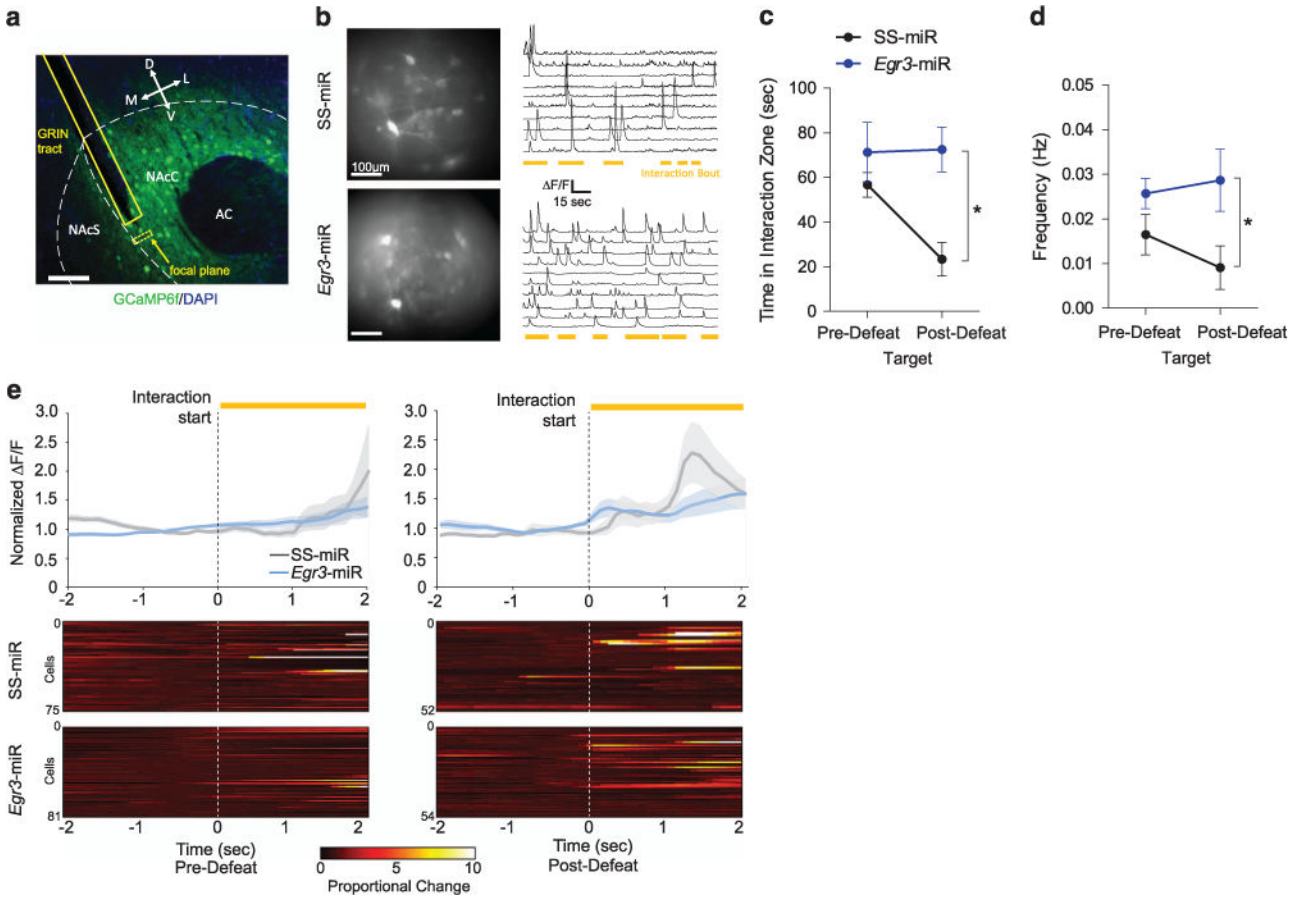


**Figure 5.**

Social defeat stress reduces the frequency of NAc D1-MSN calcium transients, an effect blocked by *Egr3* knockdown. (**a**) Confocal image representing GRIN lens tract and GCaMP6f expression in the NAc of D1-Cre mice. (**b**) Max intensity images displaying representative examples of active NAc cells and ΔF/F traces in SS-miR and *Egr3*-miR mice. (**c**) Mice expressing SS-miR, but not *Egr3*-miR, displayed a significant reduction in interaction time after defeat relative to pre-defeat SI (Target: $P<0.05$; No target: $P>0.05$; $n$ = 3–4 mice per group). (**d**) *Egr3*-miR blocked the reduction in frequency of calcium transients ($F_{1,5} = 6.048$, $P<0.05$; $n$ = 3–4 mice per group). (**e**) Average normalized ΔF/F amplitude showing calcium activity 2 s prior to the start of a social interaction bout. SS-miR mice display increased average calcium transient amplitude following an interaction bout after defeat, but not before defeat. Calcium transient magnitude is increased above baseline following the start of social interaction after defeat in SS-miR mice only. For individual time statistics see Supplementary Tables 2 and 3. Exact statistics can be found in Supplementary Table 1.